https://doi.org/10.1016/j.conbuildmat.2020.121609

Circular Fibre-Reinforced Polymer (FRP)-Concrete-Steel Hybrid Multitube Concrete Columns: Compressive Behaviour

Chun-Wa Chan[a]; Shi-Shun Zhang[b, *]; Tao Yu[c]

Abstract: This paper presents a study on circular fibre-reinforced polymer (FRP)-concrete-steel hybrid multitube concrete columns (MTCCs), which consists of an outer FRP tube, a number of inner small steel tubes to form a "steel wall" and concrete filled in the remaining spaces. The advantages of MTCCs include excellent axial load and deformation capacities, ease of construction, elimination/mitigation of difficulties in transporting and installing large steel tubes, and possibility of optimising the arrangement of the small steel tubes to improve structural performance. A total of 7 pairs of MTCCs, 4 pairs of concrete-filled FRP tubes (CFFTs), 4 pairs of concrete-filled steel walls (CFSWs) and 3 pairs of concrete-filled steel tubes (CFSTs) were tested in the present study, with the investigated parameters covering the thickness of FRP tube, the number and type of steel inner tubes, the type of concrete and status of the steel inner tubes. The test results lead to an in-depth understanding of the behaviour of MTCCs under axial compression. Furthermore, a comparison between the test results and predictions by a model previously proposed by the authors shows that the model can reasonably well predict the axial load-strain behaviour of MTCCs but largely underestimates the ultimate strain of the specimen. This model may be used for conservative design, while further investigation is needed for the development of a more accurate model.

Keywords: hybrid column, confinement, FRP, steel, multitube, concrete, rubber concrete

---

[a]PhD Candidate, School of Civil, Mining and Environmental Engineering, Faculty of Engineering and Information Sciences, University of Wollongong, Wollongong, NSW 2522, Australia.

[b]Professor, School of Civil Engineering and Mechanics, Huazhong University of Science and Technology, Wuhan, Hubei, China, 430074. (corresponding author), E-mail address: shishun@hust.edu.cn

[c]Professor, Department of Civil and Environmental Engineering, The Hong Kong Polytechnic University, Hong Kong, China.

1.0 INTRODUCTION

Fibre-reinforced polymer (FRP) composites have been more and more popularly used as an alternative to traditional construction materials in civil engineering over the past decades [1-3]. FRP composites can be used not only in the strengthening of existing structures but also in the construction of new structures [4,5]. In particular, novel hybrid FRP-based structural members have attracted increasing worldwide attention over the past two decades [6,7]. Among these novel FRP-enabled structural members, a number of different forms of hybrid FRP-concrete-steel columns (e.g., FRP-concrete-steel double-skin tubular columns and FRP-confined concrete-filled steel tubes), which are featured with a combined use of FRP, concrete and steel to optimise the mechanical performance of the columns, have been proposed and studied [7-14]. In a hybrid FRP-concrete-steel column, the FRP outer tube serves as not only a confining device for enhancing the behaviour of concrete but also a stay-in-place formwork for casting concrete and a protective skin for concrete and steel against the environmental attacks. The concrete in the hybrid column can be well confined by both the FRP outer tube and the steel section, and meanwhile the local buckling of steel section can be prevented/delayed due to the restraint from the FRP tube/jacket and surrounding concrete. As a result, a better performance in terms of both load and deformation capacities can be achieved in such columns [7,10-14].

Recently, a new form of hybrid columns termed FRP-concrete-steel hybrid multitude concrete columns (MTCCs), which combined the use of an FRP tube, concrete and small steel tubes, was proposed by the third author [16]. A typical MTCC consists of an FRP outer tube, a number of small steel inner tubes to form a "steel wall", and concrete filled in the remaining spaces. Preliminary experimental and theoretical studies [16,17] have confirmed the excellent compressive behaviour of circular and square MTCCs in terms of both the axial load capacity and excellent ductility. In addition to the structural performance, several remarkable advantages can be achieved, including (1) relatively low maintenances due to the well-protected concrete and steel, and (2) cost-effectiveness due to eliminated concrete formwork and reduced cost for manufacture, transportation and installation of large and heavy steel section by using standard small-scale steel tube products. More detailed information on the expected advantages of MTCCs can be found in Yu et al. [16]. In addition, a preliminary analytical model was proposed by Yu et al. [16] for predicting the axial load-strain behaviour of circular MTCCs.

In the first ever experimental study on circular MTCCs, which was presented in Yu et al. [16] with the aim to demonstrate the structural concept of the column, the number of specimens, and thus the studied parameters were relatively limited. In particular, the number of steel inner tubes in the MTCCs tested by Yu et al. [16] was only three or four, which is not typical of expected practical applications of the column form and may result in relatively non-uniform lateral confinement on concrete, especially for the concrete outside the steel tubes.

On the other hand, the use of rubber particles recycled from waste tyres to partially replace aggregate in producing concrete has attracted increasing research attention. Disposal of end-of-life tyres is a global challenge due to their long decomposing time and relatively large volume. The use of rubber aggregate in the concrete mix, however, leads to a number of issues such as significant reduction in the compressive strength and stiffness of concrete, depending on the grading and replacement ratio of rubber aggregate [18-21], as well as early cracking within the concrete due to the poor bonding between the rubber and the paste matrix [22]. Due to these disadvantages, rubber concrete has so far been limited to the non-structural use, such as landing filling and road bases. The weaknesses of rubber concrete, however, may be minimised when it is used in a confined concrete column such as CFFTs and MTCCs. Chan et al. [21] experimentally demonstrated the excellent structural performance of FRP-confined rubber concrete, and proposed an analysis-oriented model for predicting the stress-strain behaviour of such concrete with a rubber replacement ratio of up to 75%.

Against the above background, this paper presents a more comprehensive experimental study into the compressive behaviour of circular MTCCs with a wider range of section configurations, in order to achieve an improved and in-depth understanding on their mechanism. The effects of number, dimensions and status (hollow or solid) of steel inner tubes, volume ratio of steel, thickness of FRP tube and type of concrete on the compressive behaviour of MTCCs were studied through the experimental program. Importantly, the use of rubber concrete in MTCCs was examined in the present study, where the mixture design of the rubber concrete presented in Chan et al. [21] was adopted. The use of rubber concrete in MTCCs provides a possible approach to overcome the disadvantages of using end-of-life tyre rubber in producing concrete (e.g., compressive stiffness and load capacity). Finally, the analytical model proposed by Yu et al. [16] was adopted to predict the axial load-strain behaviour of the MTCCs with normal concrete in the present study. For the predictions of the

MTCCs with rubber concrete, the revised model proposed by Chan et al. [21] was adopted to properly consider the unique features of rubber concrete.

2.0 EXPERIMENTAL PROGRAM

2.1 Test specimens

In total, 34 specimens were tested under axial compression, including seven pairs of MTCCs (Figs. 1a-e), three pairs of CFFTs (Fig. 1f), four pairs of concrete-filled steel walls (CFSWs) (Figs. 1g-i) and three pairs of concrete-filled steel tubes (CFSTs) (Figs. 1j-l). Each CFSW specimen consists of a number of steel tubes to form a circular steel wall, with concrete cast inside as well as surrounded by the tubes, while each CFST specimen consists of a single steel tube with concrete cast inside. CFFTs, CFSWs and CFSTs were designed to experimentally examine the confinement mechanism in MTCCs. Each pair of specimens includes two nominally identical specimens, leading a total of 17 different cross-sectional configurations in the experimental program. All MTCC and CFFT specimens had a nominal diameter of 203 mm (outer diameter of the concrete section) and a height of 600 mm, and all CFSW and CFST specimens had the same height as the MTCC specimens. The arrangement of steel tubes in CFSW specimens was the same as that in the corresponding MTCC specimens for ease of comparison. The studied parameters included the number of steel inner tubes (i.e., 1 tube, 7 tubes, and 9 tubes), the dimensions of steel inner tubes (i.e., Type A, B and C), the thickness of FRP (i.e., 1.5 mm and 3 mm), type of concrete (i.e., conventional concrete and rubber concrete), and hollow or solid section inside the steel inner tubes. The details of the specimens are summarised in Table 1.

Each specimen in Table 1 is given a name for ease of reference. The name of MTCCs starts with four capital letters “MTCC”, followed by a number (1, 7 or 9) to represent the number of steel inner tubes and a capital letter (“A”, “B” or “C”) to represent the type of steel tubes, two capital letters (“SN”, “SR” or “HN”) to represent the status of the steel tube (“S” and “H” stand for the solid and hollow section of steel inner tubes, respectively) and the type of concrete (“N” and “R” stand for normal concrete and rubber concrete, respectively), a number (1.5 or 3.0) to represent the thickness of FRP tube (in mm), and finally a Roman number (“I” or “II”) to differentiate two nominally identical specimens of each configuration. The name of CFST or CFSW starts with four capital letters (“CFST” or “CFSW”), followed by a similar nomenclature to MTCCs, except that the two capital letters (i.e., “SN”, “SR” or

"HN") are replaced by a single capital letter ("N" or "R") to represent the type of concrete and the number of FRP thickness (i.e., 1.5 or 3.0) is removed (no FRP in CFST and CFSW specimens). For example, MTCC-9B-1.5-HN-II refers to the second specimen of the two nominally identical MTCC specimens, which have nine hollow steel inner tubes of type B, a 1.5 mm FRP tube and normal concrete. CFSW-7A-N-I refers to the first specimen of the two nominally identical CFSW specimens, which have seven type A steel inner tubes and normal concrete.

2.2 Material properties

Two types of concrete (i.e., normal concrete and rubber concrete) were used in the present study. The normal concrete was ordered from a local ready-mix concrete supplier with a maximum aggregate size of 10 mm, and the slump value measured before casting the concrete was 215 mm. The rubber concrete was produced in the laboratory following the procedure reported in Chan et al. [21], and the mix design is shown in Table 2. The replacement ratio of fine aggregates in terms of volume was chosen to be 50%, with a target strength similar to that of the normal concrete used in the present study. Due to the relatively small spaces in the specimens, cautions were taken during the casting process to minimise the bubbles/voids inside concrete. To obtain the material properties of unconfined concrete, three standard concrete cylinders (a height of 300 mm and a diameter of 150 mm) were prepared and tested for each type of concrete in accordance with AS 1012.9 [23]. The average elastic modulus E_c, concrete strength f'_{co} and the axial strain at peak stress ε_{co} were found to be 26.2 GPa, 34.5 MPa and 0.00232, respectively, for the normal concrete. For the rubber concrete, the results are 25.7 GPa, 31.8 MPa and 0.00235, respectively. For the steel tubes, tensile tests were conducted on steel coupons (three coupons for each type of steel tubes), in accordance with BS 18 [24]. These coupons were all cut from the same batch of steel tubes and had a dog bone shape with an effective width and length of 20 mm and 200 mm, respectively. The key mechanical properties of steel averaged from the three tensile coupon tests are listed in Table 3. In addition to the tensile coupon tests, two bare steel tubes with a height of 600 mm were also tested under axial compression for each type of steel tubes to obtain the axial stress-strain behaviour of the bare steel tubes. The obtained compressive stress-strain curves of all bare steel tubes are plotted in Fig. 2, in which typical buckling modes of the bare steel tubes are also shown for comparison purposes.

2.3 Specimen preparation

The preparation of MTCC specimens started with cutting the steel tubes into the designed height and then placing them to form a circular steel tube wall with a temporary holder. Point electric arc welding was employed to the two ends of the steel tubes to secure the tubes in the desired configurations. Three steel rods were horizontally attached to each end of the steel tube wall by point electric arc welding to ensure that they were concentrically located in the specimen. Strain gauges were next attached to the steel tubes at proper positions before casting concrete. For MTCC specimens with hollow steel tubes, the steel tube was filled with the Styrofoam at the upper end to avoid the infilling of concrete. During the concrete casting, particular caution employing tamping rod together with vibrator was taken to minimise the voids inside the column, especially for the section with small space. The Styrofoam was removed after several days' curing of concrete. A photo of concrete formwork is shown in Fig. 3. Lastly, the regions near the two ends of the specimen were each wrapped by an additional 2-layer GFRP sheet of a 30 mm width to avoid local failure at the column ends. It should be noted that the point welding and the additional layers of GFRP were limited to the two ends of the specimens and thus had little effect on the mid-height region of the specimens.

2.4 Test set-up

A pair of LVDTs (i.e., LVDTs-1&2 in Fig. 4) were applied opposite to each other along the circumference of the specimens to capture the axial displacement between the two loading plates. Another pair of LVDTs (i.e., LVDTs-3&4 in Fig. 4) were applied opposite to each other along the circumference of the specimens to measure the shortening of the 200 mm segment at the mid-height of the specimen. In addition, extensive strain gauges were applied to capture the local strain development of the specimens during the test. Figs. 5a and b show the layout of strain gauges attached at the mid-height of the specimens, while Fig. 5c shows a 360-degree external view of the strain gauges arrangement on the FRP tube. In total, strain gauges at three different heights of the specimen (i.e., one-quarter height from either of the two ends and mid-height) were used for the FRP outer tube to examine the hoop strain distribution, as shown in Fig. 5c.

All tests were carried out using a general compression-testing machine with a load capacity of 5000 kN, with the load being applied at a displacement rate of 0.6 mm/min. A steel cap with gypsum was used at each end of the test specimen to ensure uniform loading across the entire end section of the test specimen. A data logger is employed to record all test data (displacement, strains and loads).

3.0 FAILURE MODES

3.1 MTCCs and CFFTs

All MTCC and CFFT specimens failed by the rupture of the FRP tube with noticeable noise. The 360-degree external view of the first specimen (i.e., the specimen "I") of the two nominally identical ones for each configuration of MTCCs and CFFTs is shown in Fig. 6, which is produced by merging multiple photos from different angles. The tests of these specimens were all terminated at the first explosive rupture of FRP tube in the hoop direction (followed by a sudden drop of the axial load). It can be seen from Fig. 6 that the MTCC specimens with a thinner FRP outer tube (t_{frp} = 1.5 mm) show much more axial failure on the FRP outer tube (i.e., more cracks in or close to the hoop direction) (Figs. 6a-e) than the CFFT specimen (Figs. 6g and h) due to the larger ultimate axial strain of the former. The length of FRP rupture region (represented by the dashed line in Fig. 6) in the MTCC specimens with a thinner FRP outer tube is much larger than that of the corresponding CFFT specimens (Figs. 6a-h), while the MTCC and CFFT specimens with a thicker FRP outer tube had similar lengths of FRP rupture region (Figs. 6i and j). To explore the reason for the above different observations, the hoop strains at quarter heights and at mid-height of the specimen are plotted in Fig. 7, in which the hoop strain at quarter heights is averaged from eight strain gauges at the upper and lower quarter heights (see Fig. 5c) while that at mid-height is averaged from four strain gauges at the mid-height (also see Fig. 5c). It can be seen from Fig. 7 that the hoop strain at the quarter height is consistently lower than that at mid-height for all specimens, because an additional FRP wrap was used at each end of the specimens to avoid possible failure therein. It can also be seen from Fig. 7a that the above strain gap in CFFTs with a 3.0 mm FRP tube is smaller than those with a 1.5 mm FRP tube, this is because the thickness of the additional FRP warp near the end was the same for all specimens and thus the non-uniformity of the confinement along the height caused by the additional FRP wrap is relatively smaller for specimens with a thicker FRP tube (i.e., 3.0 mm FRP tube in the present study). Therefore, the rupture of FRP in CFFTs with a 3.0 mm FRP tube spread longer along the height (Fig. 6i). It can be seen from Fig. 7b that for the hoop strain gap in MTCCs with a 1.5 mm FRP tube is very small, this is because in addition to FRP tubes, the steel inner tubes also provided additional confinement to concrete and thus the influence of the end additional

FRP wrap on the non-uniformity of the confinement along the height of the specimen is relatively small in MTCCs. Therefore, the rupture of FRP tube in all MTCCs happened in a large region along the height.

For each configuration of MTCCs and CFFTs, the second specimen (i.e., the specimen “II") was deliberately further loaded after the failure of the specimen (i.e., after the first hoop rupture of FRP) to examine its residual load. The tests of the second MTCC specimens were all terminated at the second significant load drop occurred while the second CFFT specimens were all terminated at reaching 75% of load reduction. The axial load-shortening curves of Specimens MTCC-7A-SN-1.5-I, II and CFFT-1.5-N-II are plotted in Fig. 8 as examples to show the post-failure behaviour of the specimen. The LVDTs located at the mid-height 200 mm region (i.e., LVDTs-3&4) experienced impacts from the explosive rupture of FRP tube and could not be function well afterwards, therefore the average reading from LVDTs-1&2 (the overall shortening of the specimens) is used to plot the curves in Fig. 8. It should be noted that the shortening reading at the initial stage (before axial shortening of 2 mm) overestimated the actual shortening of the column due to the small gaps between the specimen and the two loading plates, resulting in a slightly non-linear curve at the initial stage. It can be seen from Fig. 8 that the first FRP rupture of the CFFT specimen occurred at the axial shortening of 13.6 mm, followed by a slight load drop. At the axial shortening of 14.1 mm, the CFFT specimen completely lost its structural integrity. In contrast, after the failure of Specimen MTCC-7A-SN-1.5-II, the specimen can still take a certain level of load (approximately 80%-90% of the load corresponding to the transition region of the axial load-shortening curve), due to the existence of the embedded steel tube wall. This residual load showed only a slight decrease as the axial shortening increased from 21.8 mm to 26.8 mm, after which the load dropped from approximately 1700kN to 1500kN due to the complete rupture of FRP tube outside the reinforced end regions.

3.2 CFSTs and CFSWs

The failure modes of the CFST and CFSW specimens are shown in Fig. 9, from which it can be seen that most specimens failed in a combination of overall buckling and local buckling (i.e., Figs. 9a-f), while Specimen CFST-1C-N-I failed in a local buckling mode (Fig. 9g) due to its low height-to-diameter ratio (see Table 1). The key results of the CFSW and CFST specimens are summarised in Table 4, in which the nominal compressive load (N_0) is defined as the sum of the load capacity of each component (i.e., steel and concrete) and can be calculated by:

$$N_0 = A_{st}\, f_{y,st} + A_c\, f'_{co} \quad (1)$$

where A_{st} is the cross-sectional area of steel; $f_{y,st}$ is the yield stress of steel; A_c is the cross-sectional area of concrete; and f'_{co} is the unconfined concrete strength.

Fig. 10 shows the steel tubes taken out from MTCC specimens after test. No visible buckling of steel tubes was observed in the first specimen of each MTCC with solid steel inner tubes (Figs. 10a-f), indicating that the FRP outer tube and the surrounding concrete provided effective constraints to prevent the steel inner tubes from buckling. In contrast, the steel tubes in the Specimen MTCC-9B-HN-1.5-I showed inward local buckling at several positions (see Fig. 10g). In addition, the steel tubes from the second specimen of each MTCC, which was deliberately further loaded after its failure, is shown in Figs. 10h-n. For Specimen MTCC-1C-SN-1.5-II, only local buckling was observed (Fig. 10h). Mixed failure modes of different levels (i.e., overall buckling and local buckling) were observed in MTCC specimens with 7-tube and 9-tube configurations (Figs. 10i-m). The buckling of steel tubes in the above specimens is much less significant than that in their corresponding CFSW specimens (Fig. 9). It can be seen from Fig. 10n that the steel tubes in Specimens MTCC-9B-HN-II showed similar buckling failure mode with MTCC-9B-HN-1.5-I (i.e., inward local buckling at several positions), with the buckling in the second specimen being slightly severer.

To further examine the buckling behaviour of the steel inner tubes, the axial strains obtained from the strain gauges on steel inner tubes are compared with that from the LVDTs at mid-height, as shown in Fig. 11a. In the present study, the axial strains used in plotting curves were all averaged from the readings of two LVDTs located at the mid-height 200 mm region of the specimen (i.e., one third of the specimen height), unless otherwise specified. It can be seen from Fig. 11a that for most MTCC specimens with solid steel inner tubes, the axial strains from both instruments are close to each other, except for Specimens MTCC-9B-SN-1.5-I, II, in which the strain values from strain gauges are much larger than those from LVDTs. To further examine the strain behaviour of MTCC-9B-SN-1.5-I, II, the hoop strain readings at mid-height, lower quarter height and upper quarter height are plotted against axial strain in Fig. 11b. It can be seen from Fig. 11b that the hoop strain at the mid-height region is larger than that at lower/upper quarter height, indicating that the steel tubes at mid-height region possibly buckled outward during the loading process. In contrast, the hoop strain of MTCC-7A-SN-1.5-I, II is much more uniform along the height, as shown in Fig. 11c. Although visible buckling was not found by naked eyes in MTCC-9B-SN-1.5-I, II (Fig. 9d), the obtained strain readings indicate that possible slight overall buckling and/or local buckling of steel inner tubes in mid-height region of the specimens occurred during the loading process. The buckling of steel inner tubes in these specimens can be attributed to the following three reasons: (1) the relatively large height-to-diameter ratio of steel tubes, (2) the relatively large volume of concrete surrounded by the steel wall (see Table 1); and (3) the relatively low FRP confinement stiffness (i.e., a thinner FRP tube). For MTCC specimens with hollow steel inner tubes (i.e., Specimens MTCC-9B-HN-1.5-I, II), the strain values of steel tubes from strain gauges are much larger than those from LVDTs, which coincides with the observed inward local buckling of the steel tube as shown in Figs. 10g and n.

4.0 COMPRESSIVE BEHAVIOUR OF MTCCS

4.1 Axial load-strain behaviour

The axial load-strain behaviour of MTCC and CFFT specimens are plotted in Fig. 12 for comparison. It is evident that all axial load-strain curves consist of two nearly linear ascending branches and a smooth transition zone between them, with the second branch having a significantly smaller slope than the first branch. It can also be seen from Fig. 12a that the slopes of the first ascending branch of the axial load-strain curve are mainly dependent on the steel volume ratio: a larger steel volume ratio leads to a larger slope of the first ascending branch, while the slopes of the second ascending branch are almost the same for most plotted specimens in the same subfigure as the same thickness of FRP tube was adopted for these specimens. For Specimens MTCC-9B-SN-1.5-I, II, however, the slope of the second ascending branch decreases gradually with the axial strain. One of the possible reasons for this phenomenon can be the possible buckling of the steel inner tubes in these two specimens, as mentioned in Section 3.2.

The key results of CFFT and MTCC specimens are summarised in Table 5, in which the nominal compressive load (N_0) (Eq. 1) is once again employed to represent the sum of the load capacities of the components (steel and concrete) in MTCCs if they do not interact with each other and the FRP tube. It should be noted that the marginal axial load directly carried by the FRP tube is ignored in the calculation of N_0, because the thickness of the FRP tube is very small and the fibres in the FRP tube are oriented close to the hoop direction. The effectiveness of confinement can be reflected by the N_{ul}/N_0 ratio shown in Table 5, where N_{ul} is the ultimate load of the test specimen. It can be seen from Table 5 that in the MTCC specimens with 1 or 7 steel inner tubes, the concrete was effectively confined and the N_{ul}/N_0 ratio range from 1.48 to 1.70. For the specimens with 9 steel stubs inner and 1.5 mm FRP tube, the N_{ul}/N_0 ratios are relatively low (ranging from 1.26 to 1.37), due to the possible buckling of steel inner tubes as mentioned in Section 3.2.

To further investigate the axial load-strain behaviour of MTCCs, the comparison of the axial load-strain curves of MTCCs between the test results and the summations of the curves of CFFTs and bare steel tubes are plotted in Fig. 13. In this figure, the axial load of the steel is assumed to be constant after its peak load due to the fact that the steel inner tubes are well confined by the FRP outer tube. Moreover, the curves of CFFTs were modified by a reduction factor to consider the slightly different area of concrete in MTCCs because of the existence of the steel tubes. It can be seen from Fig. 13 that for the MTCC specimens with a 1.5 mm FRP tube (i.e., Figs. 13a-d), the sum curves are very similar to those of MTCCs from the test, except for the Specimens MTCC-1C-SN-1.5-I, II and MTCC-7A-SN-1.5-I, II, in which the sum curves have slightly lower slopes of the second branch (see Figs. 13a and b). For MTCC specimens with a 3 mm FRP tube, the sum curves agree very well with those from the test, as shown in Fig. 13e. It is also evident from Fig. 13 that the MTCC specimens generally have a significantly larger ultimate axial strain than the corresponding CFFT specimens.

It has been pointed out in Yu et al. [16], the axial load-strain behaviour of the MTCCs are subjected to the following counteracting effects: (1) the steel inner tubes can provide additional confinement to the concrete inside them and lead to an increase in the axial load contribution of this part of the concrete, (2) the steel tubes are subjected to both the axial compression (due to the compression load applied to the specimen) and hoop tension (due to the expansion of concrete inside them), so the direct axial load contribution from the steel tubes in MTCCs is lower compared with the uniaxial loaded hollow steel tubes; and (3) the confinement from the FRP tube to the steel inner tubes can prevent/mitigate the local buckling of the steel tubes and thus increase their contribution to the axial load. Therefore, the axial load-strain behaviour of MTCCs is relatively complicated and is dependent on not only the parameters of FRP tube (e.g., the thickness and modulus) but also the parameters of steel tubes (e.g., the diameter-to-thickness ratio, yield stress and volume ratio). For MTCC specimens in Figs. 13a-b, the enhancing effect is slightly larger than the reduction effect and thus the sum curve is lower than the curves directly from test, while for MTCC specimens in Figs. 13c-e, the reduction effect can be approximately offset by the enhancing effect and thus the sum curve agrees well with the curves directly from test.

4.2 Behaviour of CFSW in MTCC

It is not unreasonable to assume that the concrete between the FRP tube and the steel wall ($A_{c,3}$ in Fig. 1) is mainly confined by the FRP outer tube and the confinement from the steel inner tubes is marginal. Therefore, the axial stress-strain behaviour of this part of concrete is assumed to be the same as that of the corresponding CFFT specimen. Based on the above assumption, the axial load-strain curves of MTCCs are compared with the summations of the curves of CFSW (or CFST-1C if only one steel inner tube was used in the MTCC) and the concrete outside the CFSW (calculated based on the axial stress-strain curve of corresponding CFFT specimen), as shown in Fig. 14. It can be seen from Fig. 14 that the axial load-strain curves of MTCCs from the test are all much higher than the sum curves. This can be attributed to two main reasons: (1) the FRP tube effectively prevent/mitigate the buckling of the steel inner tubes and thus increase their axial contributions, and (2) the FRP tube also provide confinement to concrete inside the steel inner tube as well as concrete surrounded by the steel tube wall, but such confinement was not included in the sum curves. It can be seen from Fig. 14 that compared with MTCCs with one steel inner tube, the gaps between the two groups of curves (i.e., the sum and the MTCCs) are much more pronounced for MTCCs with 7 or 9 steel inner tubes. For MTCCs with 7 or 9 steel inner tubes, the sum curves even show a descending second branch (Figs. 14b and c). This is mainly because that the confinement from the single steel tube to concrete in CFST-1C is more effective than that from the steel tube wall to concrete (surrounded by the steel wall) in CFSW specimens as the steel tubes in the latter suffered from significant outward overall buckling (Figs. 9a-c) due to the relatively large height-to-diameter ratios (see Table 1). Such buckling is believed to have a certain effect on the confined concrete inside the steel tubes. Future study (e.g., finite element analysis) is needed for a full understanding of the concrete behaviour.

4.3 Hoop expansion of the concrete

The hoop-axial strain curves of the selected MTCC specimens are shown in Fig. 15. It is clearly shown in the figure that the curves of the MTCCs are generally similar, while the curves of the two CFFT specimens are both above those of MTCCs (i.e., higher hoop strains for a given axial strain). This is because that the steel inner tubes in MTCCs can provide additional confinement to the concrete (the part inside the steel tube and the part surrounded by the steel tube wall) and thus further restrain the expansion of concrete. In the present study, a number of strain gauges were used to measure the hoop strain developments of the steel inner tubes. The comparisons of the hoop strains between the steel inner tubes and FRP outer tube in MTCCs are shown in Fig. 16, from which it can be seen that the hoop strains averaged from the four mid-height strain gauges on the FRP outer tube of 1-tube and 7-tube MTCCs with 1.5 mm FRP tube and 9-tube MTCCs with 3.0 mm FRP tube are slightly larger or similar to that from the steel inner tube, indicating a relatively uniform expansion in the entire cross-section of MTCCs. For Specimens MTCC-9B-SN-1.5-I, II, the hoop strain of the steel inner tubes is larger than that of FRP outer tube. This might be because the hoop strain reading of the steel tubes was influenced by local buckling of the steel tubes.

5.0 EFFECTS OF COLUMN CONFIGURATION

5.1 Effects of number of steel tubes and steel volume ratio

To investigate the effect of number of steel tubes on the behaviour of the confined concrete in MTCCs, the deduction method which was used in a number of existing studies [21,25], is adopted to approximately extract the stress-strain response of the confined concrete in MTCCs. The average axial stress of the concrete in MTCCs by adopting the deduction method was calculated through the following steps: (1) subtract the axial load contribution from the corresponding steel tubes (assuming it is equal to the axial load obtained from the axial compression tests of the bare steel tubes) from the axial load of the MTCC at a given axial strain; and (2) divide the axial load obtained from Step (1) by the total cross-sectional area of the concrete. The so-obtained average axial stress of concrete versus axial strain curves of eight MTCC specimens from the present study and six specimens from the authors' previous study [16] are compared in Fig. 17. These specimens had the same cross-sectional area, same height and the same thickness of the FRP tube. The number of steel inner tubes covers 1, 3, 4, 7 and 9, and the steel volume ratio ranges from 7.02 % to 12.0 %. The details of the specimens in Yu et al. [16] is summarised in Table 6. The slope of the second branch of the axial stress-strain of concrete in MTCCs (i.e., E_2) is dependent on the confinement provided by the FRP tube as well as inner steel tubes, which can be influenced by the configuration of the steel tubes. For ease of comparison, two reference lines (dash-dot) with the same value of E_2 (i.e., 1.05 GPa) and different intercepts with the stress axis (i.e., 35MPa and 47.5 MPa) were also plotted in Fig. 17. It can be seen from Fig. 17 that the values of E_2 for all examined configurations generally agree with the reference lines, suggesting that the configuration of steel tubes in the present study (number of steel inner tube from 1 to 7 and steel volume ratio from 7.02 % to 12.0 %) only has minor effect on the slope of the second branch of the stress-strain curves of confined concrete in MTCCs. For the Specimens MTCC-9B-SN-1.5-I, II, the slopes of the second branch decrease gradually with the axial strain due to the possible buckling of steel inner tubes, as discussed in the previous sections. Due to the complex mechanism of MTCCs, advanced simulation method, such as finite element analysis, is necessary to accurately extract the stress-strain response of the confined concrete in MTCCs to further investigate the effect of column configuration.

5.2 Effect of FRP thickness and status of steel tubes

The axial load-strain curves of the six MTCC specimens having nine steel inner tubes each, but different FRP thicknesses and status (solid or hollow) of steel tubes are compared in Fig. 18. As expected, the MTCC specimens with a thicker (i.e., 3.0 mm) FRP tube (i.e., MTCC-9B-SN-3.0-I, II) have a much higher ultimate axial load and strain as well as a steeper second branch of the axial load-strain curve than the MTCC specimens with a thinner (i.e., 1.5mm) FRP tube (Fig. 18). The MTCC specimens with hollow steel inners (i.e., MTCC-9B-HN-1.5-I, II) showed lower slopes of first and second branches of the axial load-strain curves as well as a much lower ultimate load than those with solid steel tubes (i.e., MTCC-9B-SN-1.5-I, II), as shown in Fig. 18. This is mainly due to the smaller cross-sectional area of concrete and the inward local buckling of hollow steel tubes, as shown in Fig. 10g.

5.3 Effect of concrete type

To examine the applicability of the structural use of rubber concrete in MTCCs, a total of six specimens filled with rubber concrete were prepared and tested under uniaxial compression, including two MTCCs, two CFFTs and two CFSWs. Similar to the MTCCs and CFFTs with normal concrete, MTCCs and CFFTs filled with rubber concrete also failed by the rupture of FRP tube in hoop direction, as shown in Figs. 6d and h, respectively. However, it can be seen from these two figures that the rupture of the FRP tube occurred in the region between the mid-height and upper quarter height of the column. This can be attributed to the following reasons: (1) the density of rubber aggregate (870 kg/m^{3}in the present study) was much lower than that of natural aggregate (around 2500 kg/m^3), thus the rubber aggregate could move upwards during the vibration of concrete and the upper half of the specimen would have more rubber aggregates; (2) under the same axial strain, the rubber concrete has a larger lateral expansion than the normal concrete with a similar compressive strength [21] and thus incur a larger hoop strain in the upper half of the FRP tube.

The steel tubes of CFSW-9B-R-I and from the MTCC-9B-SR-1.5-I, II are shown in Figs. 9d, 10e and 10l, respectively. The buckling mode of CFSW-9B-R-I is the combination of overall and local buckling (Fig. 9d) and very similar to the CFSW-9B-N-I (Fig. 9c). For the steel inner tubes from the MTCCs with rubber concrete, similar to the MTCC with the same configuration and normal concrete (Fig. 10d), no visible buckling is observed, as shown in Fig. 10e. For the MTCC-9B-SR-1.5-II, which was further loaded after the first rupture of FRP tube, the buckling mode is also similar to the MTCC with normal concrete (Fig. 10k) but the location of the outward bending shifted upward to between the mid-height and upper quarter height of the specimen (Fig. 10l). This might be also attributed to the non-uniform distribution of the rubber aggregate discussed previously.

To examine the hoop strain distribution along the height of the MTCCs with rubber concrete, the hoop strain readings from the three height levels (i.e., mid-height, upper and lower quarter heights) are plotted against axial strain in Fig. 19. It can be clearly seen from Fig. 19 that the maximum hoop strain occurred at upper quarter height while the minimum hoop strain occurred at the lower quarter of height for both MTCC specimens, agreeing well with the observed failure mode of these two specimens. Thus, the hoop strain readings from upper quarter height of CFFT-N-1.5-I, II and MTCC-9B-SR-1.5-I, II are selected to represent the hoop expansion of the specimens in the following discussion.

Fig. 20 shows the hoop-axial strain relationships of the CFFTs and MTCCs with rubber and normal concrete. It can be seen from Fig. 20a and 20b that for a given axial strain, the hoop strains in specimens (either CFFTs or MTCCs) with rubber concrete are higher than those in specimens with normal concrete at upper quarter height of specimen, which is consistent with the findings in Chan et al. [21] that the rubber concrete has a larger lateral expansion than normal concrete at the same axial strain of the specimen. The comparison of hoop-axial strain curves at the failure locations of specimens (i.e., mid-height for specimens with normal concrete, while upper quarter height for specimens with rubber concrete) shows that the hoop strains at upper quarter height of CFFTs with rubber concrete are slightly higher than those at mid-height of CFFTs with normal concrete, while the hoop strains at upper quarter height of MTCCs with rubber concrete are similar/slightly lower than those at mid-height of MTCCs with normal concrete. The above phenomenon is believed to at least due to the following two counteracting effects: (1) specimens with rubber concrete should have a larger hoop strain than specimens with normal concrete at the same axial strain, due to the larger expansion of rubber concrete [21]; and (2) specimens should normally have a smaller hoop strain at upper quarter height than at the mid-height, as the concrete at the upper quarter height (150 mm from the specimen end) may be still affected by the lateral restraint from the specimen end. In the present study, the first effect appears larger for CFFTs, while the second effect appears larger for MTCCs. This might be due to the complex interactions between FRP, concrete and steel tubes of MTCCs. Further research is required to examine the strain behaviour of rubber concrete in the hybrid FRP-steel-concrete columns.

The comparison of axial load-strain curves between MTCCs with rubber concrete and normal concrete is shown in Fig. 21, from which it can be seen that the axial load-strain curves of MTCCs with normal concrete have nearly the same shape as well as the same slope of the second branch as those of MTCCs with rubber concrete. However, the axial loads of the MTCCs with rubber concrete are slightly lower than those of MTCCs with normal concrete for a given axial strain, as shown in Fig. 21. This is believed to be attributed to the lower unconfined concrete strength of rubber concrete (31.8MPa), compared to the normal concrete on the present study (34.5 MPa). It can be seen from Fig. 21 that the ultimate axial strains of MTCCs with rubber concrete are higher than those with normal concrete. This is at least partially due to the larger average rupture strain of FRP in MTCCs with rubber concrete than that in MTCCs with normal concrete, as can be seen from Table 5. Although more studies are needed in the future to gain an in-depth understanding on behaviour (especially the hoop-axial strain behaviour) of MTCCs with rubber concrete, the present study well demonstrates that the rubber concrete with a replacement ratio of up to 50% can be employed in MTCCs to achieve an acceptable structural behaviour.

6.0 THEORETICAL MODELLING

Yu et al. [16] proposed an analytical model for predicting the axial load-strain curves of MTCCs, making use of Teng et al.'s analysis-oriented model [26] for CFSTs and Jiang and Teng's analysis-oriented model [27] for CFFTs. Yu et al.'s model [16] was adopted for the prediction of MTCCs with normal concrete in the present study.

The comparison between the experimental and predicted axial load-strain curves is shown in Fig. 22. It is not surprising that for all MTCCs, the ultimate axial strain was considerably underestimated. This is because that the ultimate axial strain of the corresponding CFFTs is simply used for MTCCs, according to Yu et al. [16]. Despite this, it can be seen from Figs. 22b and c that the axial load-axial strain curves of MTCCs with steel tubes of type B and 1.5 mm FRP tube (i.e., MTCC-7B-SN-1.5-I, II and MTCC-9B-SN-1.5-I, II) can be reasonably predicted by Yu et al.'s model [16]. The predictions are also reasonable for Specimens MTCC-7A-SN-1.5-I, II and MTCC-1C-SN-1.5-I, II, although a slight underestimation of the second branch of the curve was observed (Figs. 22a and d). This might be because that in these specimens the cross-sectional area of concrete inside the steel tubes are relatively large, and the FRP confinement to this part of concrete is ignored in Yu et al.'s model [16]. For the Specimen MTCC-9B-SN-3.0-I, II, the model also slightly underestimates the axial load in the later stage (i.e., after axial strain of 0.03), as shown in Fig. 22e. This might also be because of the neglect of FRP confinement to the concrete inside the steel tube, considering that the error caused by such neglect may become noticeable when the FRP tube is relatively thick (e.g., for Specimen MTCC-9B-SN-3.0-I, II).

For MTCCs with rubber concrete, Yu et al.'s model [16] for the MTCC with normal concrete is first adopted and shown as Prediction-I in Fig. 22f. Due to the unique feature of rubber concrete, Prediction-I appears to underestimate the axial load at the transition point. To better capture the features of rubber concrete, the approach proposed by Yu et al. [16] was adopted, but with a revised analysis-oriented model for CFFTs to account for the unique characteristics of FRP-confined rubber concrete. In doing so, the following two components of Jiang and Teng's model [27] were revised: (1) the peak axial stress equation of active confinement model; and (2) the equation for the hoop strain-axial strain behaviour. The equations which were developed in Chan et al. [21] based on the test results of FRP-confined rubber concrete, were adopted for the above two components, respectively. The so-obtained prediction is also shown in Fig. 22f (Prediction-II). It can be seen that Prediction-II provides a closer prediction of the axial load-strain curves, although it significantly underestimates the ultimate axial strain, due to the oversimplification of the method as discussed above (i.e. simply using the ultimate axial strain of the corresponding CFFTs for MTCCs). Nevertheless, the above discussions suggest that the approach proposed by Yu et al. [16], with modifications to address the unique properties of rubber concrete, can be used for a conservative design of MTCCs.

7.0 CONCLUSIONS

This paper presents the results of axial compression tests on the circular MTCCs with 1-tube, 7-tube and 9-tube configurations. The test programme included a total of 14 MTCCs and 20 other related columns (i.e., CFFTs, CFSWs and CFSTs) for comparison, with the studied parameters covering the thickness of FRP tube, the number and type of steel inner tubes, and the status of the steel inner tube. The use of rubber concrete in MTCCs was also examined for the first time. The test results presented in this paper extended the understanding of the compressive behaviour of circular MTCCs, and lead to the following conclusions:

1) The rupture of the FRP tube in MTCCs was found to be more evenly distributed along the height of the specimen than that in CFFTs, indicating a more uniform hoop expansion of concrete along the height of MTCCs. The buckling of steel tubes happened in CFST specimens can be well prevented or mitigated in MTCCs, leading to a higher axial load contribution from steel tubes in MTCCs than in CFSTs.
2) Compared with the corresponding CFFTs, the MTCCs have a higher ultimate load as well as a larger ultimate axial strain, due to the existence of steel tubes inside. In general, a larger steel ratio leads to a higher ultimate axial load.
3) The hoop strain reading obtained from the steel inner tube was found to be slightly smaller or similar to that obtained from the FRP outer tube in MTCCs, indicating a relatively uniform lateral expansion over the cross-section of an MTCC.
4) The MTCCs with hollow steel tubes showed much inferior performance than MTCCs with solid steel tubes, due to the smaller cross-sectional area of concrete and the inward local bucking of the inner hollow steel tubes.
5) The MTCCs with rubber concrete (with a fine aggregate replacement ratio of 50%) achieved excellent structural performance which is comparable to MTCCs with normal concrete. MTCCs thus provide an excellent opportunity for the structural applications of rubber concrete.

The analysis approach proposed by Yu et al. [16] has also been shown to provide reasonable predictions of the axial load-strain behaviour of MTCCs with normal concrete. With modifications to address the unique dilation behaviour of rubber concrete [21], this approach can also predict reasonably well the axial load-strain curves of MTCCs with rubber concrete. Yu et al.'s [16] approach, however, generally considerably underestimates the ultimate axial strain of MTCCs due to its oversimplified assumptions. While Yu et al.'s approach [16] may be used for conservative design, it does not reflect the complex interaction mechanism of the three constituent materials (FRP, concrete, steel) of MTCCs. Three-dimensional finite element modelling needs to be conducted to explicitly simulate the interaction between the three materials and to reveal the confinement mechanism of the column, based on which a more rational and reliable design approach should be developed.

ACKNOWLEDGEMENT

The authors are grateful for the financial support provided by the Australian Research Council (Project ID: DP170102992).

REFERENCES

[1] Teng, J. G., Chen, J. F., Smith, S. T. and Lam, L. (2002) *FRP Strengthened RC Structures*, John Wiley & Sons, Ltd.

[2] Uddin, N. (Ed.). (2013). *Developments in fiber-reinforced polymer (FRP) composites for civil engineering*. Elsevier.

[3] Yan, L., Kasal, B. and Huang, L. (2016). "A review of recent research on the use of cellulosic fibres, their fibre fabric reinforced cementitious, geo-polymer and polymer composites in civil engineering" *Composites Part B: Engineering*, 92, 94-132.

[4] Fam, A. Z. and Rizkalla, S. H. (2001). "Behavior of axially loaded concrete-filled circular fiber-reinforced polymer tubes", *ACI Structural Journal*, 98(3), 280-289.

[5] Hollaway, L. C. (2010). "A review of the present and future utilisation of FRP composites in the civil infrastructure with reference to their important in-service properties", *Construction and Building Materials*, 24(12), 2419-2445.

[6] Lam, L. and Teng, J. G. (2003). "Design-oriented stress-strain model for FRP-confined concrete", *Construction and Building Materials*, 17(6-7), 471-489.

[7] Karimi, K., Tait, M. J. and El-Dakhakhni, W. W. (2011). "Testing and modelling of a novel FRP-encased steel-concrete composite column", *Composite Structures*, 93(5), 1463-1473.

[8] Yu, T., Lin, G. and Zhang, S. S. (2016). "Compressive behavior of FRP-confined concrete-encased steel columns", *Composite Structures*, 154, 493-506.

[9] Idris, Y. and Ozbakkaloglu, T. (2016). "Behaviour of square fibre reinforced polymer-high-strength concrete-steel double-skin tubular columns under combined axial compression and reversed-cyclic lateral loading", *Engineering Structures*, 118, 307-319.

[10] Huang, L., Yu, T., Zhang, S. S. and Wang, Z. Y. (2017). "FRP-confined concrete-encased cross-shaped steel columns: Concept and behaviour", *Engineering Structures*, 152, 348-358.

[11] Guo, Y. C., Ye, Y. Y., Lv, J. F., Bai, Y. L. and Zeng, J. J. (2020). "Effective usage of high strength steel tubes: Axial compressive behavior of hybrid FRP-concrete-steel solid columns", *Thin-Walled Structures*, 154, 106796.

[12] Guo, Y. C., Xiao, S. H., Shi, S. W., Zeng, J. J., Wang, W. Q. and Zhao, H. C. (2020). "Axial Compressive Behavior of Concrete-Filled FRP-Steel Wire Reinforced Thermoplastics Pipe Hybrid Columns", *Composite Structures*, 112237.

[13] Zeng, J. J., Lv, J. F., Lin, G., Guo, Y. C. and Li, L. J. (2018). "Compressive behavior of double-tube concrete columns with an outer square FRP tube and an inner circular high-strength steel tube", *Construction and Building Materials*, 184, 668-680.

[14] Zhang, Y., Wei, Y., Bai, J., Wu, G. and Dong, Z. (2020). "A novel seawater and sea sand concrete filled FRP-carbon steel composite tube column: Concept and behaviour", *Composite Structures*, 112421.

[15] Teng, J. G., Yu, T., Wong, Y. L. and Dong, S. L. (2007). "Hybrid FRP–concrete–steel tubular columns: concept and behavior", *Construction and Building Materials*, 21(4), 846-854.

[16] Yu, T., Chan, C. W., Teh, L. and Teng, J. G. (2017). "Hybrid FRP-Concrete-Steel Multi-Tube Concrete Columns: Concept and Behaviour", *Journal of Composites for Construction*, ASCE, 21(6), 04017044.

[17] Chan, C. W, Yu, T. and Zhang, S. S. (2018). "Compressive behaviour of square fibre-reinforced polymer-concrete-steel hybrid multi-tube concrete columns", *Advances in Structural Engineering*, 21(8), 1162-1172.

[18] Eldin N. N. and Senouci A. B. (1993). "Rubber-tire particles as concrete aggregate", *Journal of Materials in Civil Engineering*, 5(4), 478-496.

[19] Khaloo A. R., Dehestani M. and Rahmatabadi P. (2008). "Mechanical properties of concrete containing a high volume of tire–rubber particles", *Waste Management*, 28(12), 2472-2482.

[20] Moustafa A. and ElGawady M. A. (2015). "Mechanical properties of high strength concrete with scrap tire rubber", *Construction and Building Materials*, 93, 249-256.

[21] Chan, C. W., Yu, T., Zhang, S. S. and Xu, Q. F. (2019). "Compressive behaviour of FRP-confined rubber concrete", *Construction and Building Materials*, *211*, 416-426.

[22] Ganjian E., Khorami M. and Maghsoudi A. A. (2009). "Scrap-tyre-rubber replacement for aggregate and filler in concrete", *Construction and Building Materials*, 23(5), 1828-1836.

[23] AS1012.9 (2014). "Compressive strength tests- concrete, mortar and grout specimens", *Method of Testing Concrete,* Standards Australia.

[24] BS18 (1987). "Method for tensile testing of metals (including aerospace materials)", British Standards Institution.

[25] Wong, Y. L., Yu, T., Teng, J. G. and Dong, S. L. (2008). "Behavior of FRP-confined concrete in annular section columns", *Composites Part B: Engineering*, 39(3), 451-466.

[26] Teng, J. G., Hu, Y. M. and Yu, T. (2013). "Stress-strain model for concrete in FRP-confined steel tubular columns", *Engineering Structures*, 49, 156-167.

[27] Jiang, T. and Teng, J. G. (2007). "Analysis-oriented stress-strain models for FRP–confined concrete", *Engineering Structures*, 29(11), 2968-2986.

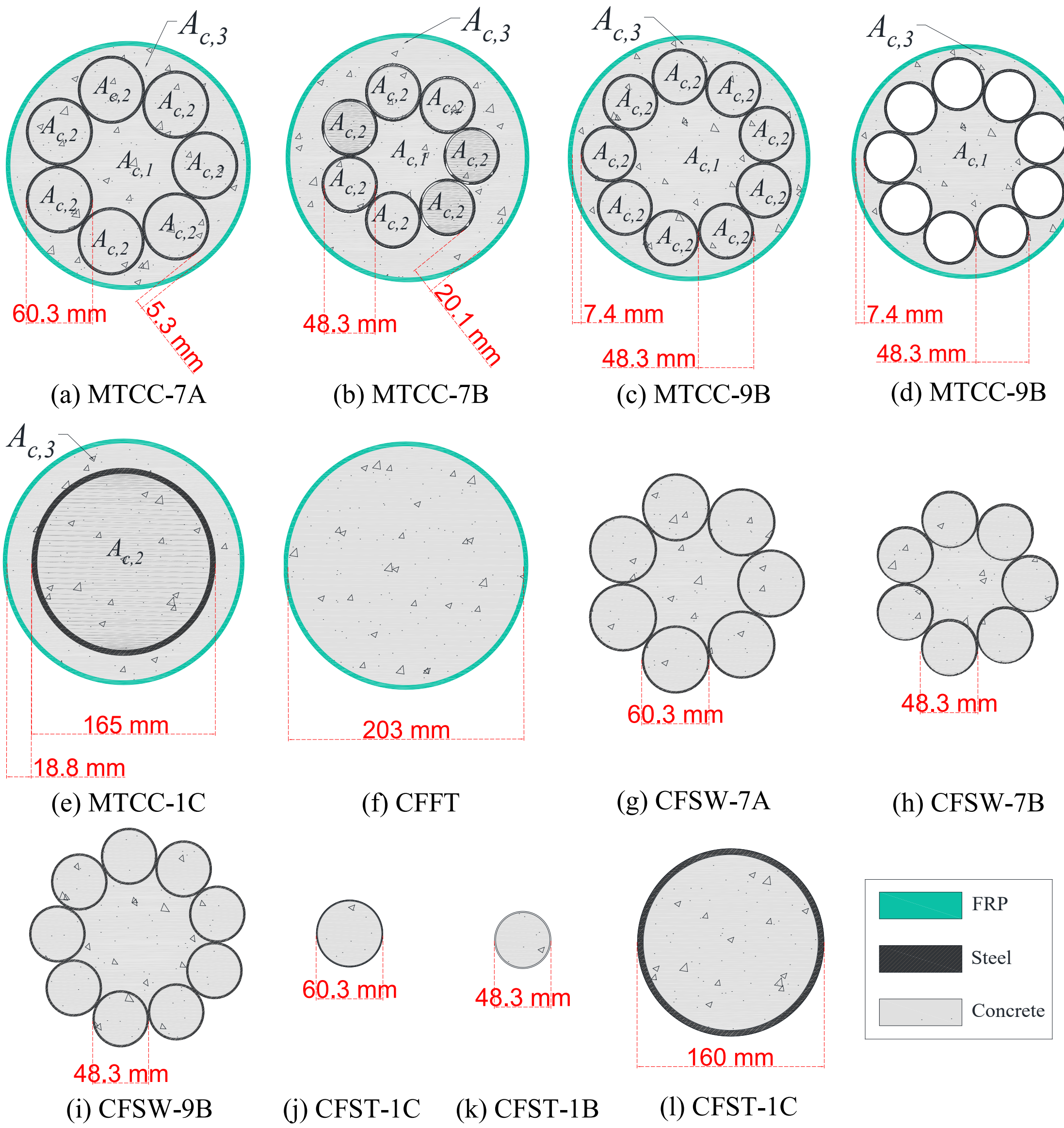

Fig. 1 Cross-sections of all specimens

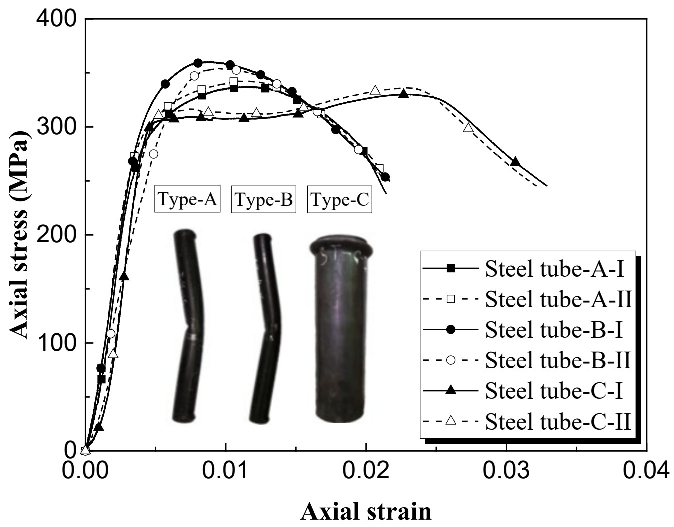

Fig. 2 Axial stress-strain curves of bare steel tubes

Fig. 3 Formwork for casting concrete

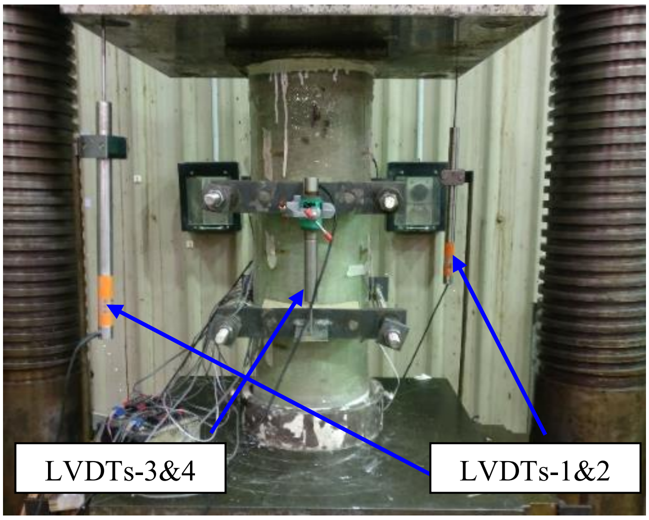

Fig. 4 Test set-up

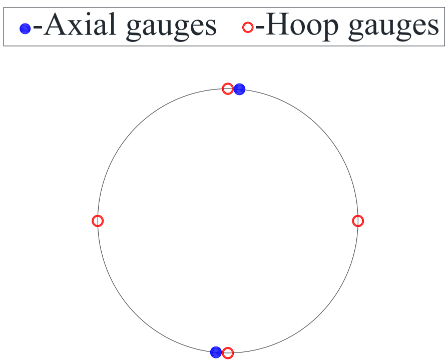

(a) FRP tube at mid-height

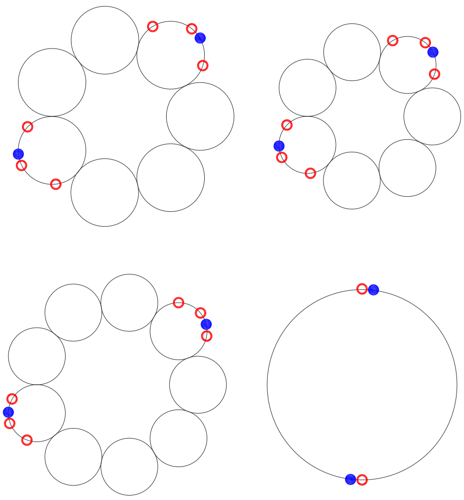

(b) steel tubes at mid-height

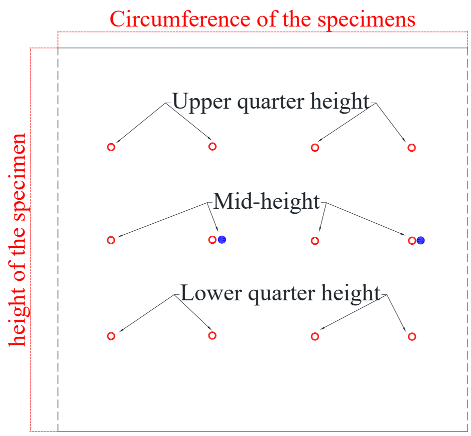

(c) 360-degree view of FRP tube

Fig. 5 Layout of strain gauges

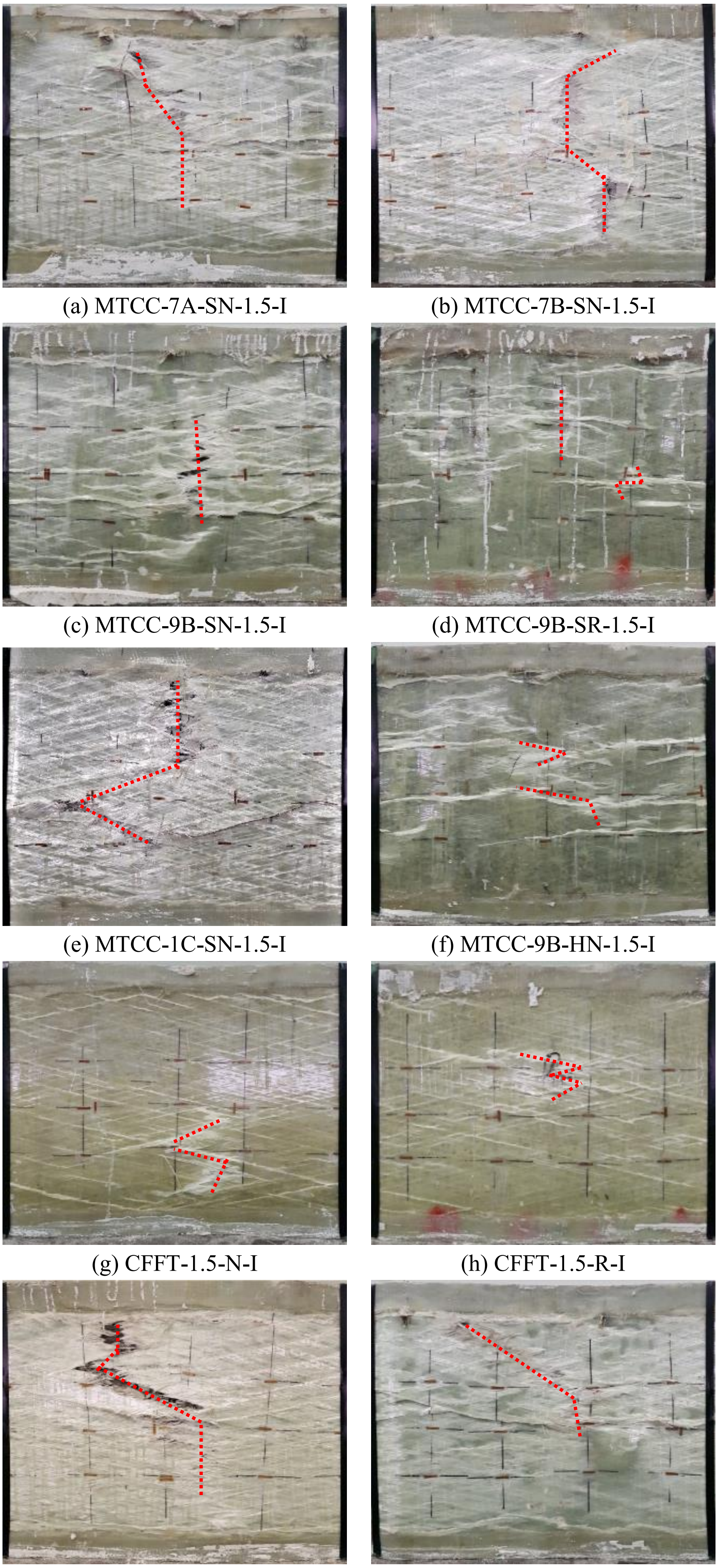

(a) MTCC-7A-SN-1.5-I (b) MTCC-7B-SN-1.5-I
(c) MTCC-9B-SN-1.5-I (d) MTCC-9B-SR-1.5-I
(e) MTCC-1C-SN-1.5-I (f) MTCC-9B-HN-1.5-I
(g) CFFT-1.5-N-I (h) CFFT-1.5-R-I
(i) CFFT-3.0-N-I (j) MTCC-9B-SN-3.0-I

Fig. 6 Failure modes of MTCCs and CFFTs (360-degree view)

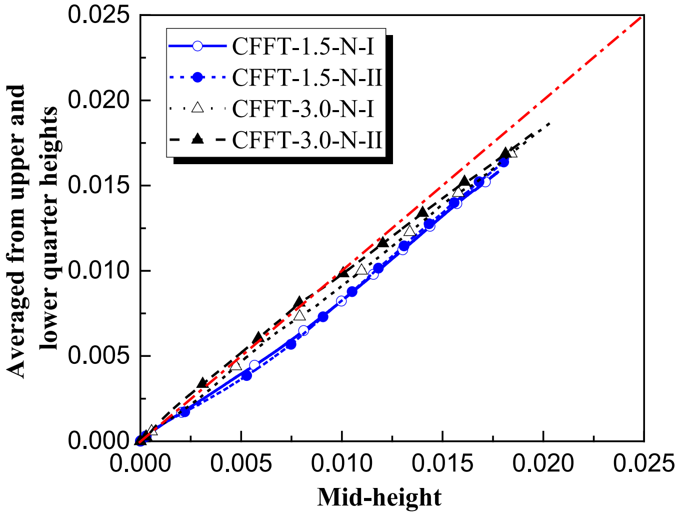

(a) CFFTs with variation of FRP thickness

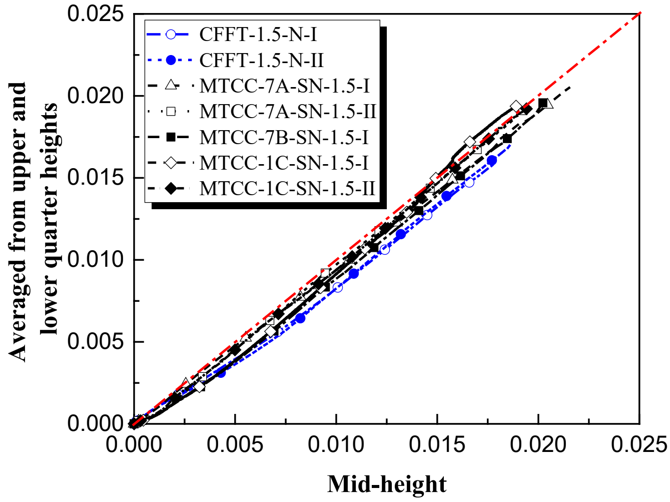

(b) CFFTs and MTCCs with the same FRP tube

Fig. 7 Comparison of hoop strains at different heights

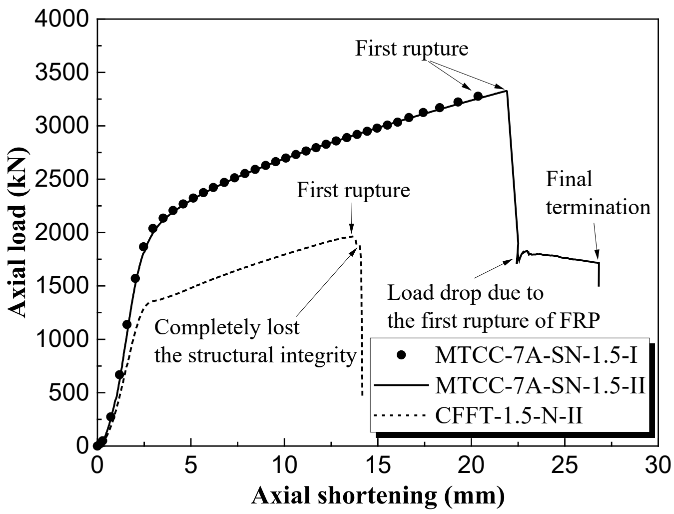

Fig. 8 Axial load-shortening curves of MTCC-7A-SN-1.5-I, II and CFFT-1.5-N-II

(a) CFSW-7A-N-I (b) CFSW-7B-N-I (c) CFSW-9B-N-I (d) CFSW-9B-R-I

(e) CFST-1A-N-I (f) CFST-1B-N-I (g) CFST-1C-N-I

Fig. 9 Failure modes of CFSTs and CFSWs

(a) MTCC-1C-SN-1.5-I (b) MTCC-7A-SN-1.5-I (c) MTCC-7B-SN-1.5-I (d) MTCC-9B-SN-1.5-I (e) MTCC-9B-SR-1.5-I (f) MTCC-9B-SN-3.0-I (g) MTCC-9B-HN-1.5-I

(h) MTCC-1C-SN-1.5-II (i) MTCC-7A-SN-1.5-II (j) MTCC-7B-SN-1.5-II (k) MTCC-9B-SN-1.5-II (l) MTCC-9B-SR-1.5-II (m) MTCC-9B-SN-3.0-II (n) MTCC-9B-HN-1.5-II

Fig. 10 Steel tubes from MTCCs after test

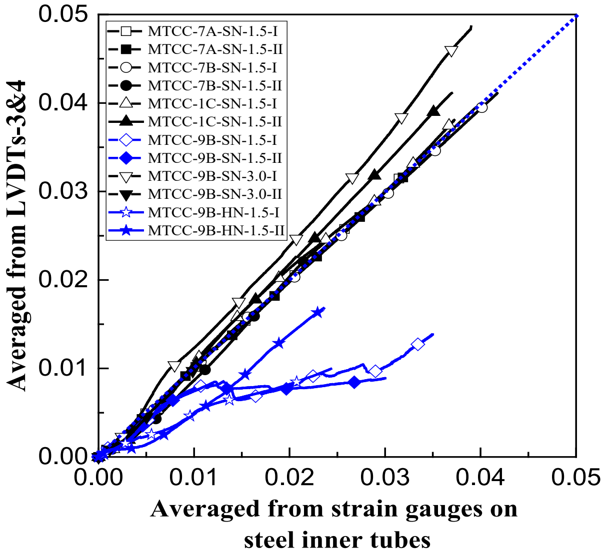

(a) Comparison of axial strains in MTCCs

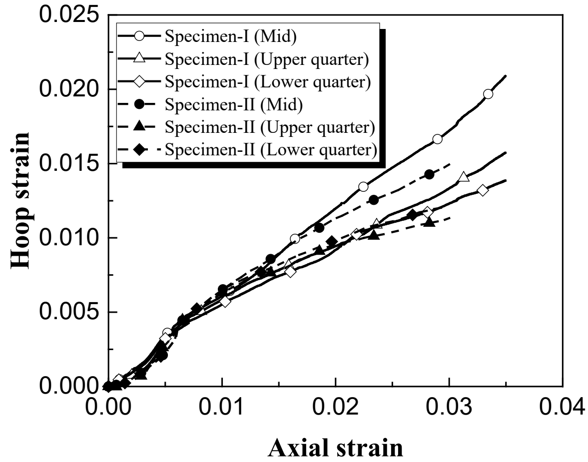

(b) Hoop-axial strain curves of MTCC-9B-SN-1.5-I, II

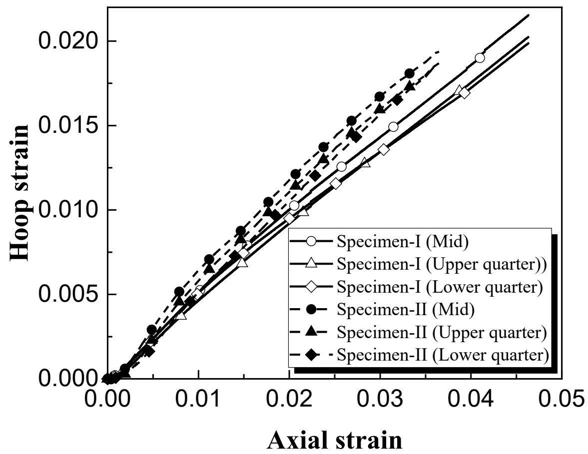

(c) Hoop-axial strain curves of MTCC-7A-SN-1.5-I, II

Fig. 11 Strain behaviour of MTCCs

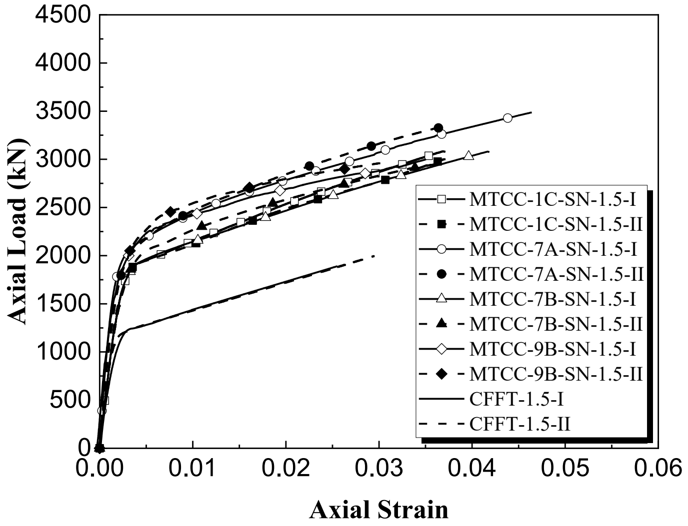

(a) MTCCs with a 1.5 mm-thick FRP tube

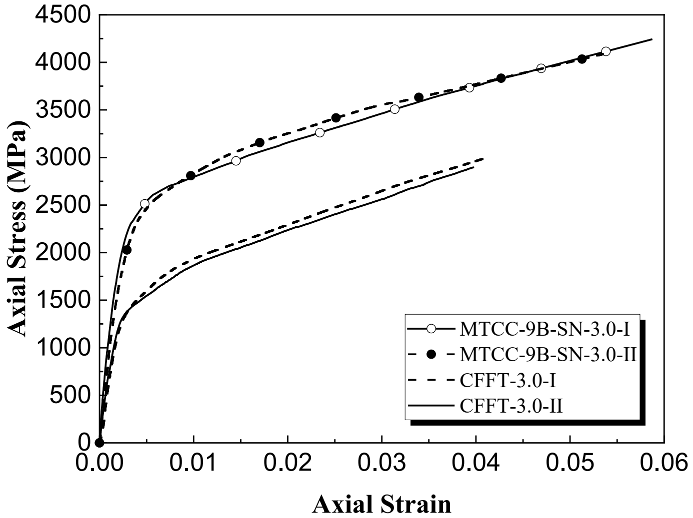

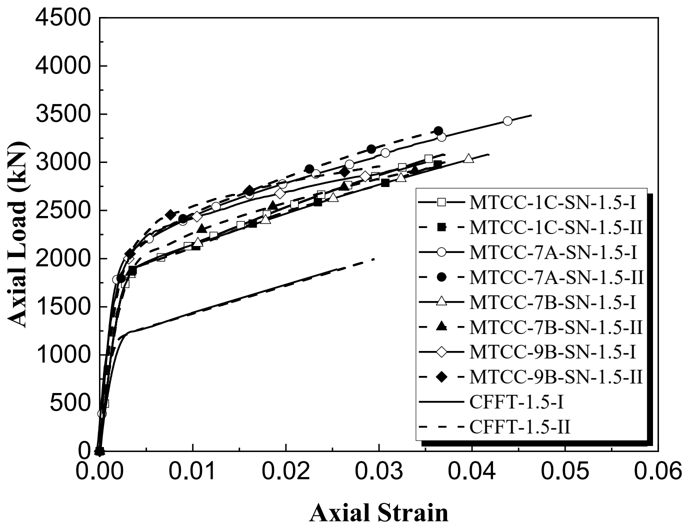

(b) MTCCs with a 3.0 mm-thick FRP tube

Fig. 12 Axial load-strain behaviour of MTCCs

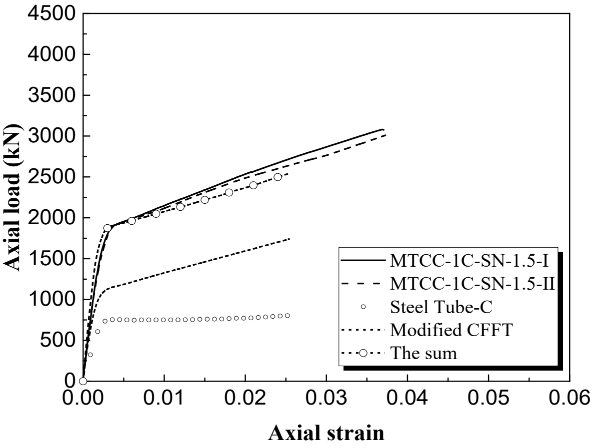

(a) MTCC-1C-SN-1.5-I,II

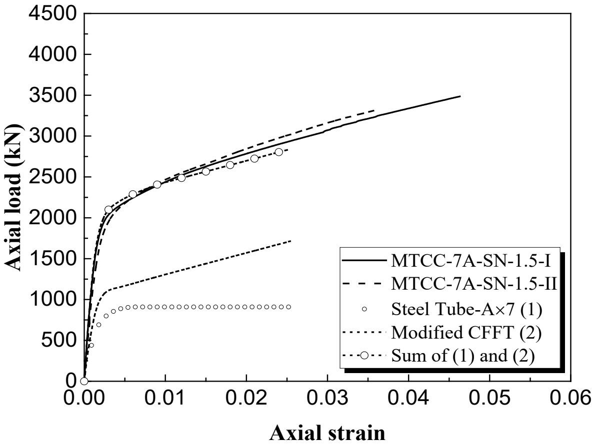

(b) MTCC-7A-SN-1.5-I,II

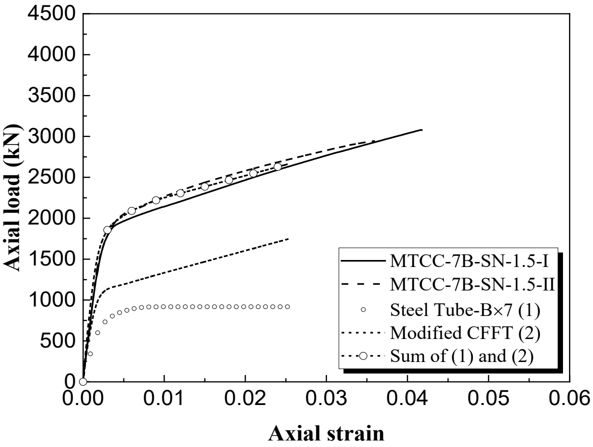

(c) MTCC-7B-SN-1.5-I,II

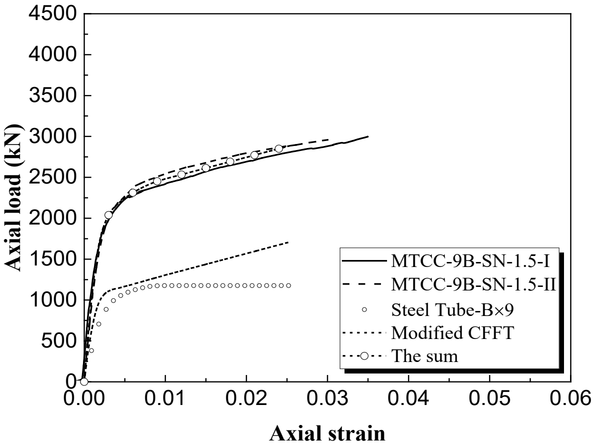

(d) MTCC-9B-SN-1.5-I,II

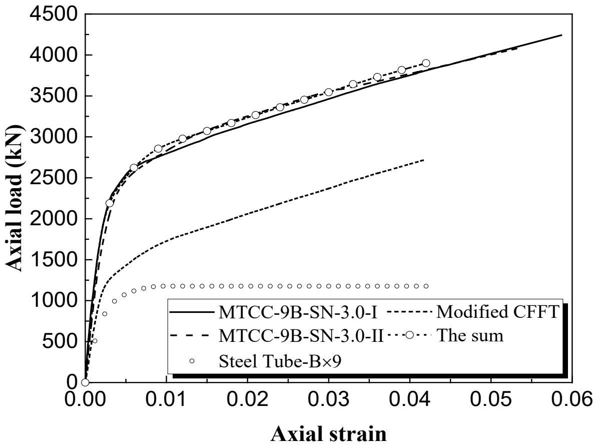

(e) MTCC-9B-SN-3.0-I,II

Fig. 13 Comparison of axial load-strain curve between MTCC and the sum curve (steel tube + concrete)

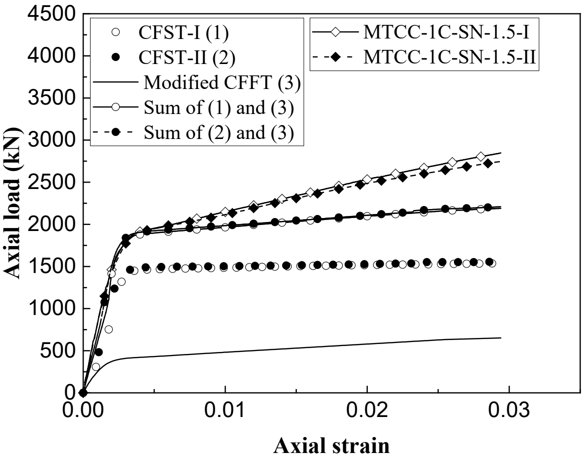

(a) MTCC-1C-SN-1.5-I, II

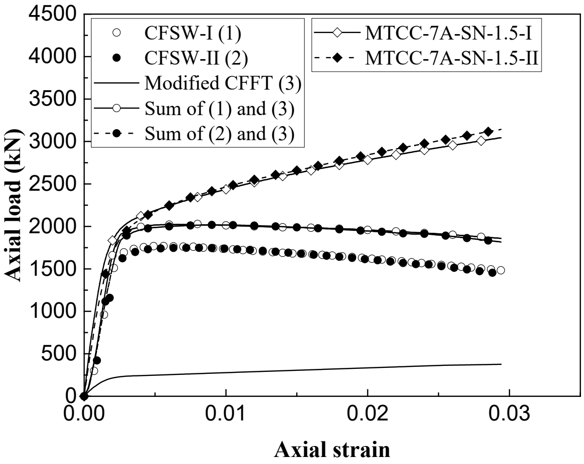

(b) MTCC-7A-SN-1.5-I, II

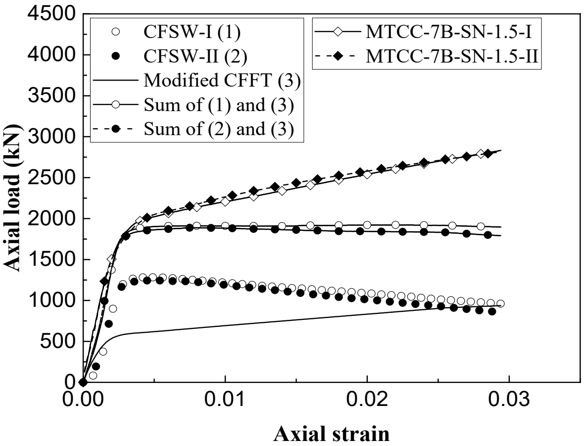

(c) MTCC-7B-SN-1.5-I, II

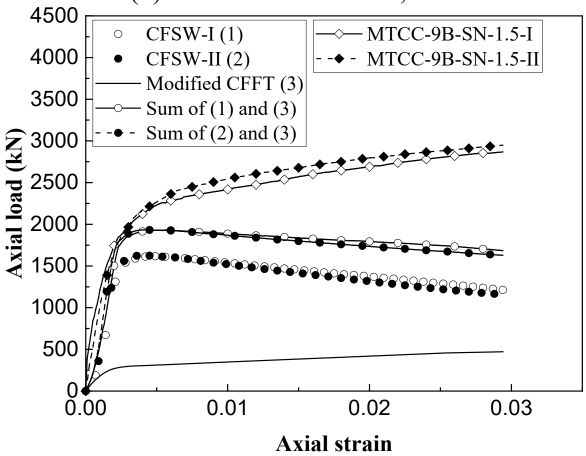

(d) MTCC-9B-SN-1.5-I, II

Fig. 14 Comparison of axial load-strain curve between MTCC and the sum curve (CFSW + concrete)

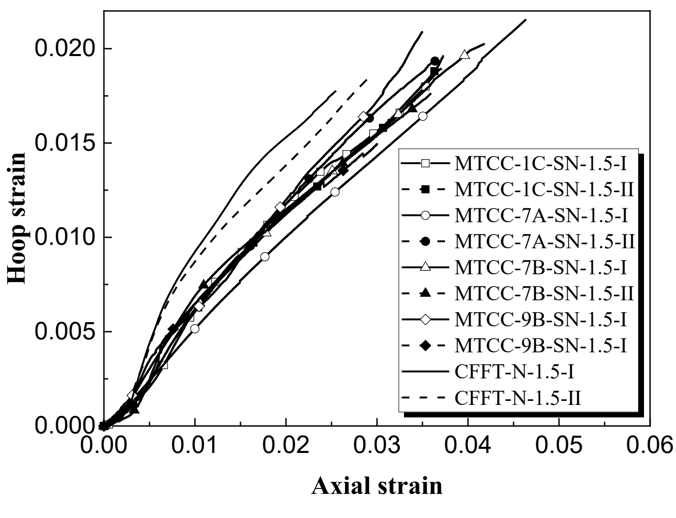

Fig. 15 Hoop-axial strain relationships of MTCCs

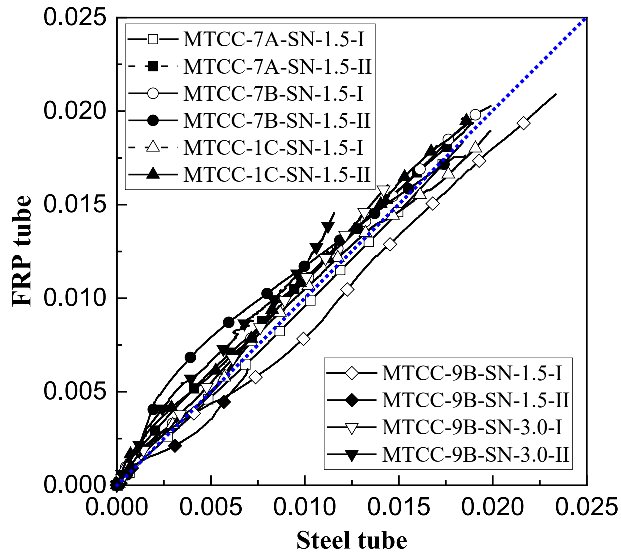

Fig. 16 Comparison of hoop strain between FRP tube and steel tube

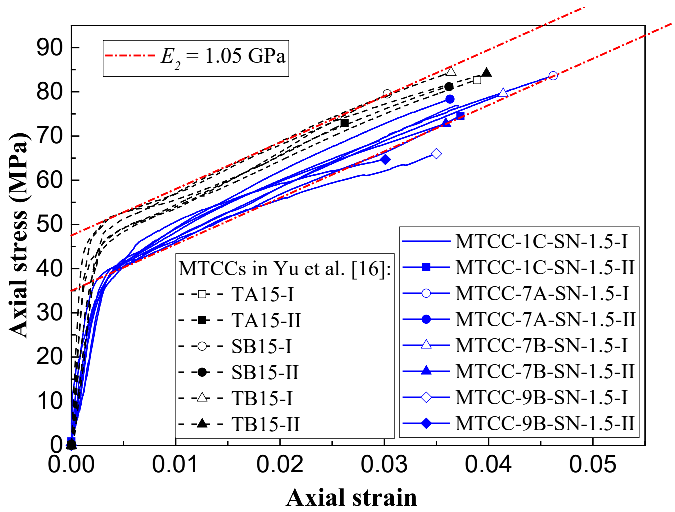

Fig. 17 Axial stress-strain curves of concrete in MTCCs

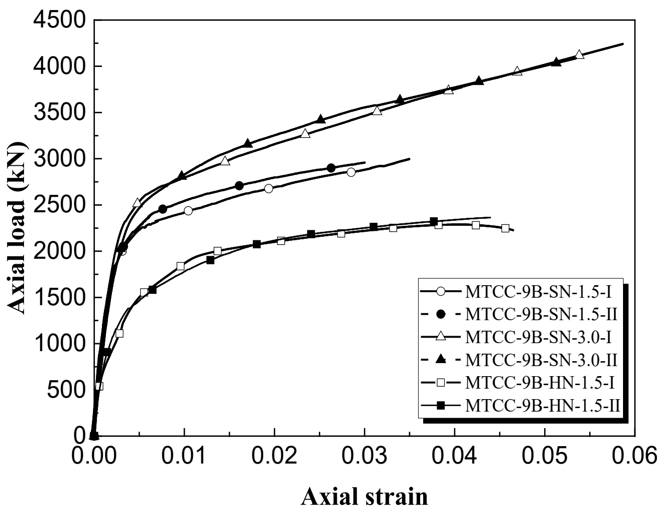

Fig. 18 Axial load-strain curves of MTCCs with 9 steel tubes

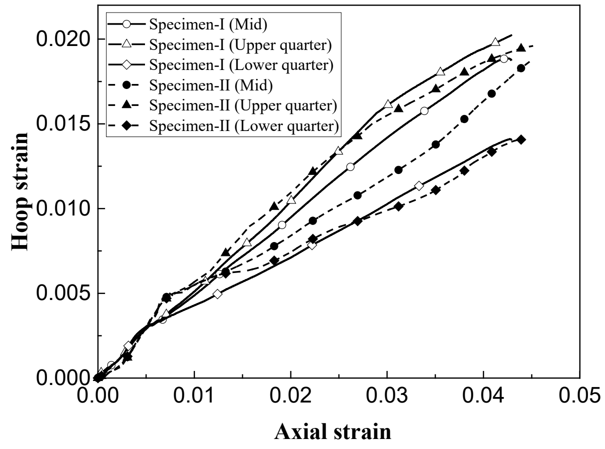

Fig. 19 Hoop-axial strain curves of MTCC-9B-SR-1.5-I, II

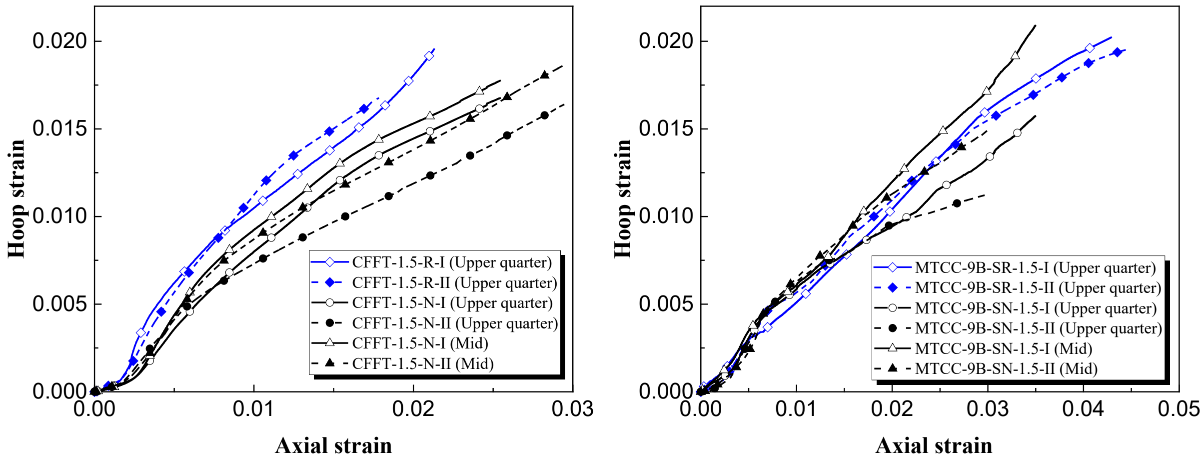

(a) CFFTs (b) MTCCs

Fig. 20 Hoop-axial strain curves

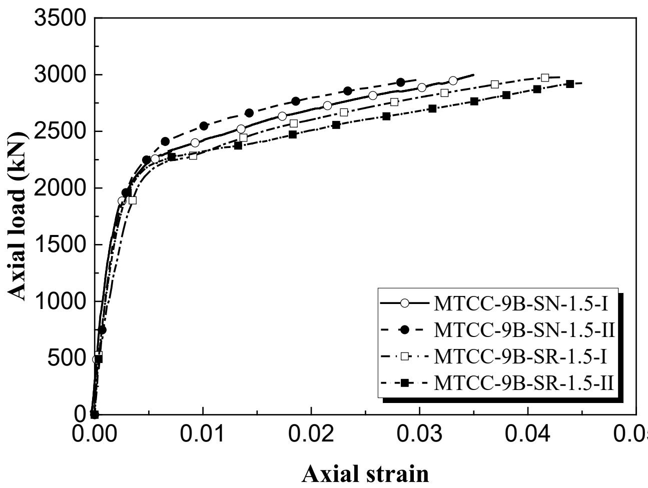

Fig. 21 Axial load-strain curves of the MTCCs with rubber and normal concrete

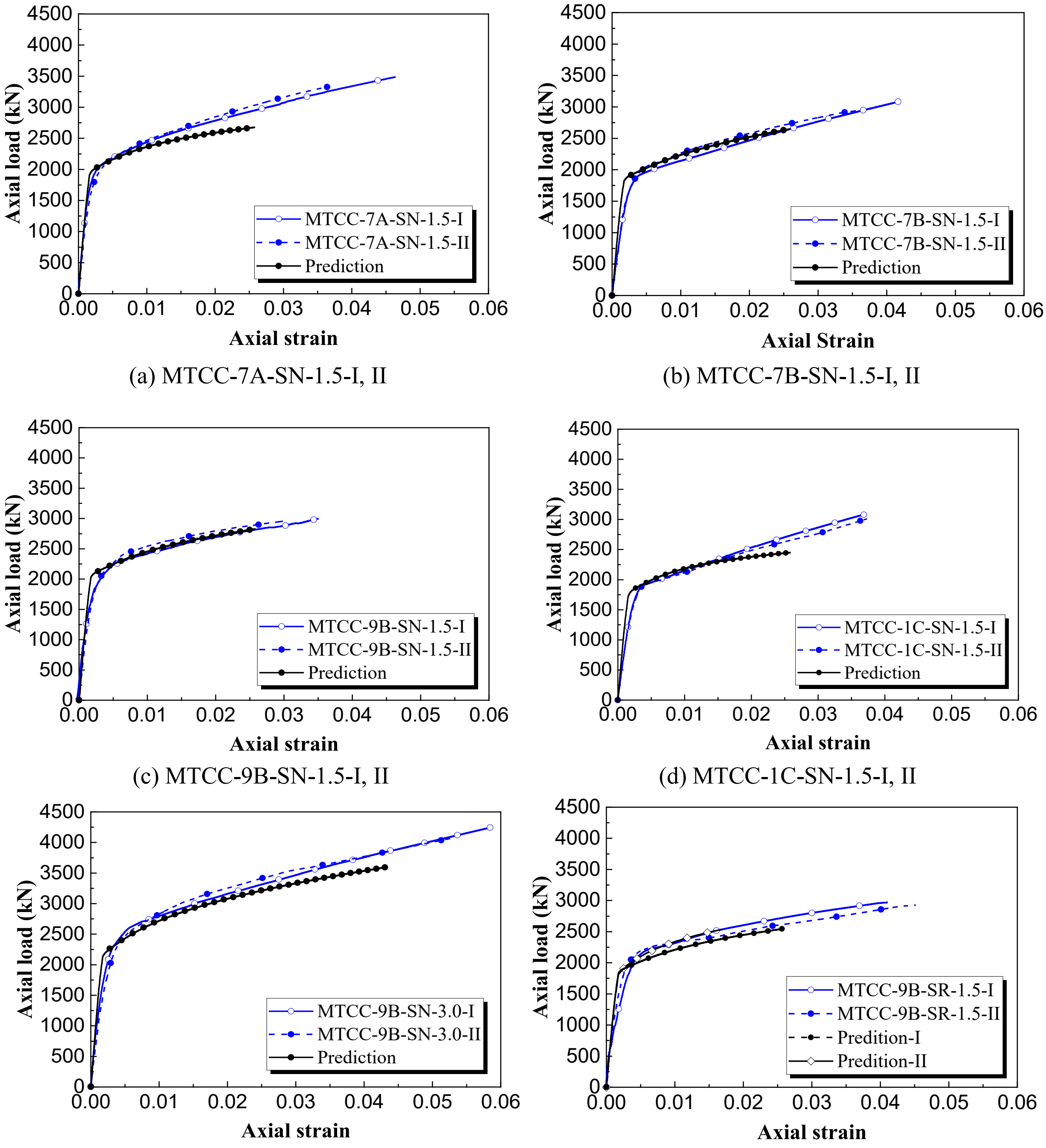

(a) MTCC-7A-SN-1.5-I, II

(b) MTCC-7B-SN-1.5-I, II

(c) MTCC-9B-SN-1.5-I, II

(d) MTCC-1C-SN-1.5-I, II

(e) MTCC-9B-SN-3.0-I, II

(f) MTCC-9B-SR-1.5-I, II

Fig. 22 Comparison of axial load-axial strain behaviour between test and prediction